How to cite: *Angew. Chem. Int. Ed.* **2023**, *62*, e202306170
doi.org/10.1002/anie.202306170

Polyoxometalates

Reversible Electrodeposition of Potassium-bridged Molecular Vanadium Oxides: A New Approach Towards Multi-Electron Storage

*Nikhil Arya[+], Tom Philipp[+], Simon Greiner, Michael Steiner, Christine Kranz, and Montaha Anjass**

Abstract: Molecular metal oxides, so-called polyoxometalates (POMs), have shown outstanding performance as catalysts and lately attracted interest as materials in energy conversion and storage systems due to their capability of storing and exchanging multiple electrons. Here, we report the first example of redox-driven reversible electrodeposition of molecular vanadium oxide clusters, leading to the formation of thin films. The detailed investigation of the deposition mechanism reveals that the reversibility is dependent on the reduction potential. Correlating electrochemical quartz microbalance studies with X-ray photoelectron spectroscopy (XPS) data gave insight into the redox chemistry and oxidation states of vanadium in the deposited films in dependence on the potential window. A multi-electron reduction of the polyoxovanadate cluster, which facilitates the potassium (K^+) cation-assisted reversible formation of potassium vanadium oxide thin films was confirmed. At anodic potentials, re-oxidation of the polyoxovanadate and complete stripping of the thin film is observed for films deposited at potentials more positive than −500 mV vs. Ag/Ag^+, while electrodeposition at more negative cathodic potential reduces the electrochemical reversibility of the process and increases the stripping overpotential. As proof of principle, we demonstrate the electrochemical performance of the deposited films for potential use in potassium-ion batteries.

Introduction

The steadily growing demand for electrochemical energy storage systems in mobile applications, grid storage, and electric vehicles is driving the need to design novel materials for effective and energy-dense electrochemical energy storage.[1] Metal oxides are chemically suitable and economically viable materials class for energy technologies including batteries,[2] fuel cells,[3] and water electrolysis.[4]

Molecular metal oxides, so-called polyoxometalates (POMs) combine physicochemical similarity to solid-state metal oxides with molecularly well-defined structures (Figure 1).[5] POMs are anionic metal oxo clusters of high-valent, early transition metals (often molybdenum (Mo), tungsten (W), and vanadium (V)), which form spontaneously in

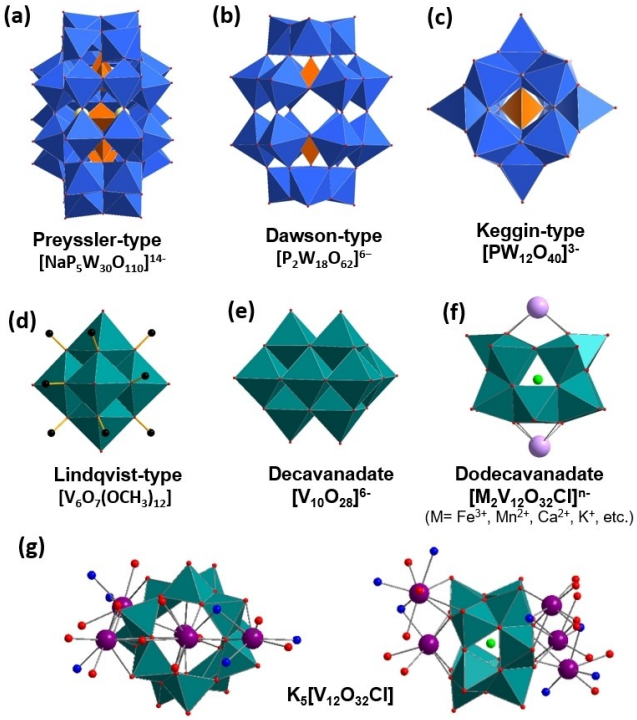

Figure 1. Polyhedral illustration of POM anions, used so far for cation —POM interaction studies. (a) Preyssler polyoxoanion, $[NaP_5W_{30}O_{110}]^{14-}$; (b) Dawson anion $[P_2M_{18}O_{62}]^{6-}$; (c) Keggin anion $[PM_{12}O_{40}]^{3-}$; (d) Lindqvist alkoxide cluster $[V_6O_7(OCH_3)_{12}]$; (e) Decavanadate anion $[V_{10}O_{28}]^{6-}$; (f) Dodecavanade anion $[V_{12}O_{32}Cl]^{n-}$; (g) top and side view of $K_5\{V_{12}\}$. Colour Scheme: W (blue); O (red), V (teal), C (clack), P (orange), Cl (green), metal coordination (pink), K (plum).

[*] N. Arya,[+] Dr. S. Greiner, M. Steiner, Dr. M. Anjass
Institute of Inorganic Chemistry I, Ulm University
Albert-Einstein-Allee 11, 89081 Ulm (Germany)
and
Helmholtz Institute Ulm (HIU)
Helmholtzstraße 11, 89081 Ulm (Germany)
E-mail: montaha.anjass@uni-ulm.de
T. Philipp,[+] Prof. Dr. C. Kranz
Institute of Analytical and Bioanalytical Chemistry, Ulm University
Albert-Einstein-Allee 11, 89081 Ulm (Germany)
[+] These authors contributed equally to this work.

solution by self-assembly.[5b] Particularly, Mo- and W-based POMs have attracted widespread attention in catalysis and sensing,[6] energy conversion and storage,[7] and increasingly as building blocks for supramolecular assemblies and nanostructured materials.[8] In contrast, molecular vanadium oxides (polyoxovanadates, POVs) have only recently gained substantial attention due to their rich electrochemistry.[9] Additionally, the targeted synthesis of heterometal-functionalized POVs has enabled systematic studies on the controlled structural[10] and electrochemical tuning[11] of POVs, which led to the application of POVs in (post-) Li-ion batteries,[12] water oxidation catalysis,[13] and as metal-oxide surface models.[14]

Recently, the interaction between alkali cations and POMs has been studied, and how these interactions can affect the structure and influence the electrochemical behavavior of POMs, especially POVs.[15] Matson and co-workers investigated the interaction of a Lindqvist-type POV alkoxide cluster ($[V_6O_7(OCH_3)_{12}]$, Figure 1d) with different hard and soft cations. Hard ions (e.g., Li^+) exhibit specific binding and strong interaction with POVs clusters, whereas softer cations (e.g., nBu_4N^+ or K^+), show non-specific binding and weaker interactions. Further, they showed that the identity and concentration of the charge compensating cations modulate the redox behavior of ($[V_6O_7(OCH_3)_{12}]$) in solution.[15a] In this context, Schimpf and co-workers demonstrated, how the concentration of charge compensating K^+ ions influences the phase of a polyoxotungstate-based coordination network using a Preyssler-type polyoxoanion, $[NaP_5W_{30}O_{110}]^{14-}$ (Figure 1a) cluster.[16] Also, the cation-controlled reversible storage of up to 18 electrons of Dawson-type polyoxotungstates (Figure 1b) in solution has recently been reported.[17]

As a final step for the deployment of POMs in technological applications, the transition from soluble species to solid materials and the immobilization on functional substrates remains a challenge. While most strategies so far focus on encapsulation or electrostatic interaction, the growth of supramolecular films enables a bottom-up approach towards functional (nano-) materials.[18] Additionally, electrochemical deposition enables controllable film growth. For example, the Keggin-type $[H_3PW_{12}O_{40}]$ (Figure 1c) was deposited on TiO_2 nanotube arrays via electrodeposition, and the deposited films were used for photocatalytic degradation of nitrobenzene.[19] Recently, Hwu and co-workers reported the electrochemical crystal growth of decavanadate-based organic-inorganic hybrids (Figure 1e).[20] The applied potential was used as the driving force for the phase nucleation and thus enabled the deposition of a polyoxometalate-organic framework (POMOF).

In recent studies, we reported the polymerization and formation of 1D chains of dodecavanadate clusters (Figure 1f) bridged with alkaline earth metal ions.[11d,21] Dodecavanadate clusters are derived from $(H_2NMe_2)_2[V_{12}O_{32}Cl]^{3-}$ ($=(H_2NMe_2)_2\{\mathbf{V_{12}}\}$), where two open binding sites are occupied by organic $(H_2NMe_2)^+$ cations. One or both placeholders can be replaced by s-,[21] d-,[22] or f-block[23] metal cations. Thereby, the magnetic, redox, catalytic, and photocatalytic properties can be tuned.

This approach was subsequently expanded by introducing K^+ ions,[21] leading to a complex 3D framework by coordination of K^+ ions inside and next to the predetermined binding site. Thereby, coordination of more than two K^+ ions was achieved leading to a cluster with the sum formula $K_5(CH_3CN)_3[V_{12}O_{32}Cl]$ ($=\mathbf{K_5\{V_{12}\}}$, Figure 1g). In contrast to earlier di-metal functionalized clusters, no reduction was required to introduce a second heterometal cation. In this current study, we investigated a possible reduction of $K_5\{V_{12}\}$ that may lead to an increased interaction between the negatively charged POM and the charge compensating K^+ cations enabling electrodeposition.

Consequently, we report here reduction-induced electrodeposition of POV-derived thin films directed by the inclusion of alkali cations. Our detailed electrochemical investigations of the underlying processes indicate a multiple electron reduction of the cluster. The electrochemical studies are accompanied by the characterization of the obtained films regarding their morphology and thickness of the deposited films.

Results and Discussion

Electrochemical characterization

Comparing $K_5\{V_{12}\}$ with related di-functionalized $\{V_{12}\}$-analogues, the fully oxidized vanadium centers as well as the complex 3D structure of $K_5\{V_{12}\}$ are the most striking differences.[21] We hypothesized that reduction of the cluster framework could increase the electrostatic attraction between the K^+ ions and the vanadate cluster. This may decrease the solubility and induce the deposition of thin films. Therefore, we investigated the electrochemical behavior of $K_5\{V_{12}\}$ in water-free, de-aerated acetonitrile (containing 0.1 M $(nBu_4N)PF_6$ as electrolyte salt, which has been used as a standard electrolyte in our previous studies.[11d] For most of the presented studies, glassy-carbon electrodes (Ø: 3 mm) have been used in a three-electrode cell configuration (with a Pt wire counter electrode and a silver wire in a glass frit, containing electrolyte solution as quasi-reference electrode). The cyclic voltammogram (CV) of $K_5\{V_{12}\}$ in a potential range of −250–500 mV vs. Ag/Ag^+ (Figure 2a) shows a reduction process that starts at −120 mV vs. Ag/Ag^+, which appears to be the reminiscence of plating behavior. Indeed, a deposited film becomes visible at the working electrode. Additionally, a sharp oxidation peak at $E_{peak} = -50$ mV vs. Ag/Ag^+ is observed suggesting stripping of the deposited material. Further reduction of the cluster is observed upon decreasing the cathodic potential to −500 mV vs. Ag/Ag^+. Moreover, a second convoluted reduction process can be identified as a shoulder, which might be related to further reduction of the already deposited film. The oxidation is shifted anodically by ~30 mV, and a new oxidative peak appears at $E_{peak} =$ 220 mV vs. Ag/Ag^+ indicating that the second reduction step decreases the reversibility and slightly increases the

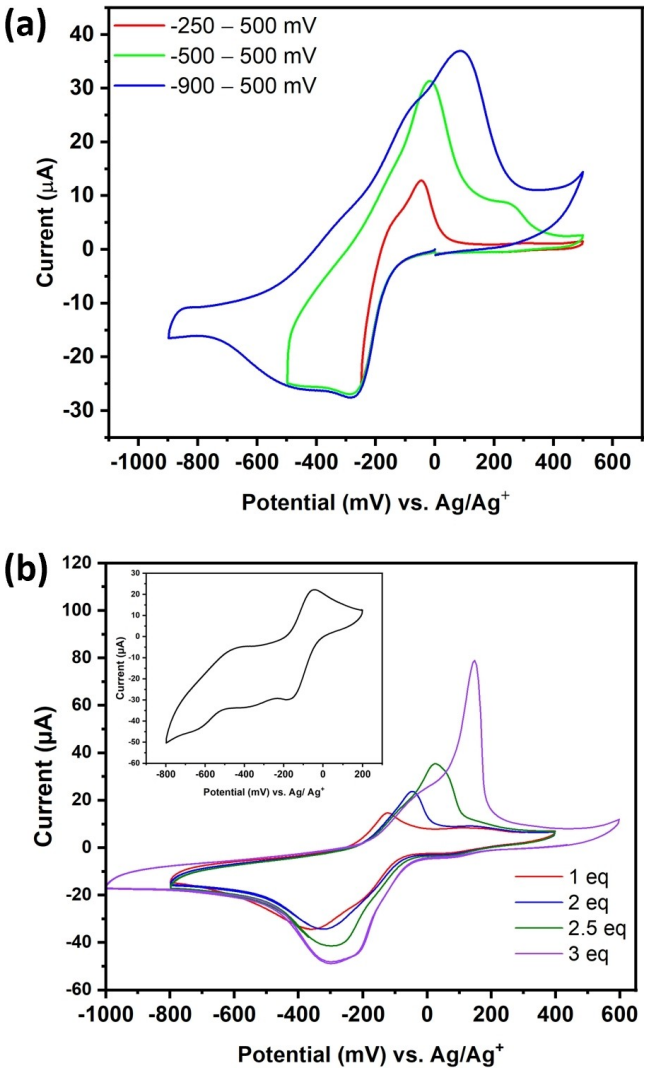

Figure 2. **a)** CVs of $K_5\{V_{12}\}$ at different cathodic switching potentials in anhydrous, de-aerated acetonitrile containing 0.1 M $(n\mathrm{Bu_4N})PF_6$ as supporting electrolyte salt, $[K_5\{V_{12}\}] = 0.5$ mM. **b)** CVs of $\{V_{12}\}$; $(H_2NMe_2)_2[V_{12}O_{32}Cl]^{3-}$ (containing 0.1 M $(n\mathrm{Bu_4N})PF_6$ as electrolyte salt) with different concentrations of KPF_6; scan rate: 100 mV s^{-1}; inset: CV of $\{V_{12}\}$; $(H_2NMe_2)_2[V_{12}O_{32}Cl]^{3-}$ in acetonitrile in absence of K+ ions.

overpotential of the stripping process. This behavior is consistent with the reduction of the cluster and associated charge compensation as the electron transfer is coupled with cation transfer, where the reduced cluster has a higher affinity for K^+ cations and is therefore more difficult to re-oxidize.

A further extension of the cathodic potential window to −900 mV vs. Ag/Ag^+ resulted in an anodic shift of the oxidation potential by 130 mV and an incomplete stripping of the deposited film. We hypothesize that at a potential lower than −500 mV vs. Ag/Ag^+, successive reduction occurs across the deposited film resulting in structural changes of the vanadate clusters stabilizing the film and affecting its stripping reversibility.

Interestingly, the CV of the non-functionalized $\{V_{12}\}$ in $(n\mathrm{Bu_4N})PF_6$ containing electrolyte shows a quasi-reversible redox process at $E_{1/2} = -150$ mV vs. Ag/Ag^+ but no electrodeposition of a film,[11d] indicating that the presence of K^+ is crucial for the electrodeposition process. These observations prompted further investigation of the electrochemical behavior of $\{V_{12}\}$ at different K^+ concentrations. The CV of the non-functionalized $\{V_{12}\}$; $(H_2NMe_2)_2[V_{12}O_{32}Cl]^{3-}$ in acetonitrile (containing 0.1 M $(n\mathrm{Bu_4N})PF_6$ as electrolyte salt) shows a quasi-reversible redox process at $E_{1/2} = -150$ mV vs. Ag/Ag^+ (Figure 2b, inset) and additional irreversible reduction processes were observed at lower potentials, indicating cluster decomposition upon further reduction. The CV changed by the addition of 1 eq KPF_6 salt, revealing a broad reduction peak centered at −350 mV vs. Ag/Ag^+ with a shoulder at ~−170 mV vs. Ag/Ag^+ and one oxidation wave at $E_{peak} = -123$ mV vs. Ag/Ag^+ (Figure 2b). Notably, the absence of irreversible reduction peaks at lower potential indicates that the presence of K^+ in solution stabilized the reduced clusters and prevented their decomposition. With addition of 2 eq K^+, a peak shift towards less cathodic potentials was observed; the subsequent additions were then resulting in an increase of the cathodic current. This indicates that the presence of more K^+ ions in solution facilitates the electrodeposition process during the reductive cycle. Further, this increase in current is also associated with a peak broadening, which may result from an overlap of multiple reduction steps of the cluster in a narrow potential range.[15a] Additionally, a shift of the oxidation peak to higher anodic potentials, in addition to an increase of anodic current is observed after each addition of KPF_6. This positive shift might be attributed to the stronger interaction between the reduced form of the cluster and K^+ ions, which reduces the electrochemical reversibility of the oxidation process.

Film electrodeposition

To further investigate the electrodeposition behavior of the $K_5\{V_{12}\}$ upon reduction as observed in the CV, bulk electrolysis (BE) was performed in a 0.5 mM acetonitrile solution of $K_5\{V_{12}\}$ (containing 0.1 M $(n\mathrm{Bu_4N})PF_6$) at −250 mV vs. Ag/Ag^+. After electrolysis (~6 h), UV/Vis spectroscopy of the bulk solution (Supporting Information, Figure S1) shows no intervalence charge transfer (IVCT) absorbance in the Vis-to-near-IR region, indicating that no detectable amounts of reduced vanadates (i.e., V^{IV}-containing) are present in the solution. At the same time, film formation was observed on the glassy carbon electrode. This provides further evidence that the reduction of $K_5\{V_{12}\}$ leads to film formation, while no reduced species are detected in the electrolyte solution, given the limit of detection (LOD) of the method.

The electrodeposition behavior and reversibility of the process were further investigated via electrochemical quartz microbalance (EQCM) analysis to determine the relation between deposited mass and transferred charge at three different potentials, i.e., −250 mV, −500 mV and −900 mV

vs. Ag/Ag^+. Applying a constant potential of −250 mV vs. Ag/Ag^+ resulted in a linear increase of deposited mass per transferred charge (Supporting Information, Figure S2). The slope of the deposited mass-to-charge ratio suggests deposition of approximately one $K_{8.64}[V_{12}O_{32}Cl]$ per 3.46 e^- (sum formula derived from XPS data).

In the next step, CVs at three different cathodic switching potentials in combination with EQCM (Figure 3a–c) were recorded. The CVs with a potential limit of −250 mV vs. Ag/Ag^+ show full reversibility with the expected plating and stripping behavior visible by the increase and decrease of the observed mass change. However, when the cathodic potential was changed to −500 mV vs. Ag/Ag^+, a deviation from the linear behavior of the transferred charge versus deposited mass was observed (Figure 3d), indicating that the deposited film was further reduced as noted by an apparent higher electron count per deposited cluster (4.9 e^- per $K_{9.36}[V_{12}O_{32}Cl]$, sum formula derived from XPS data). It should be noted that up to a lower switching potential of −500 mV vs. Ag/Ag^+ during cycling the potential, the plated films can still be completely stripped (visible in the massogram). An additional oxidative peak becomes visible, which is in line with the initial CV measurements. In case, the potential was cycled to a cathodic switching potential of −900 mV vs. Ag/Ag^+, the deposited mass per charge curve shows a significant flattening which indicates that the deposited film undergoes a further reduction as the dominant electrochemical process (6.32 e^- per $K_{11.64}[V_{12}O_{32}Cl]$, sum formula derived from XPS data). Additionally, the deposited mass was no longer fully stripped (re-oxidized) when the potential was swept anodically (to 500 mV vs. Ag/Ag^+), suggesting irreversible electrodeposition, possibly due to structural changes during further reduction. At the fifth cycle, a strong decrease in current was observed, which is in line with the absence of a frequency change, i.e., indicating that the electrode surface of the quartz sensor was blocked by an insulating film.

In the next step, pulsed electrochemical depositions (PEDs) were performed at three different potentials −250 mV, −500 mV and −900 mV vs. Ag/Ag^+, respectively, to study the influence of the reduction potential on film formation in more detail. All pulsed electrodeposition experiments were carried out in two distinct steps, the potential of 0 mV vs. Ag/Ag^+ was applied to the working electrode for 60 seconds known as relaxing period (t_{off}) to establish the bulk concentration of the dissolved cluster ions near the electrode surface. Then the desired reduction potential e.g., −250 mV vs. Ag/Ag^+ was applied for a period

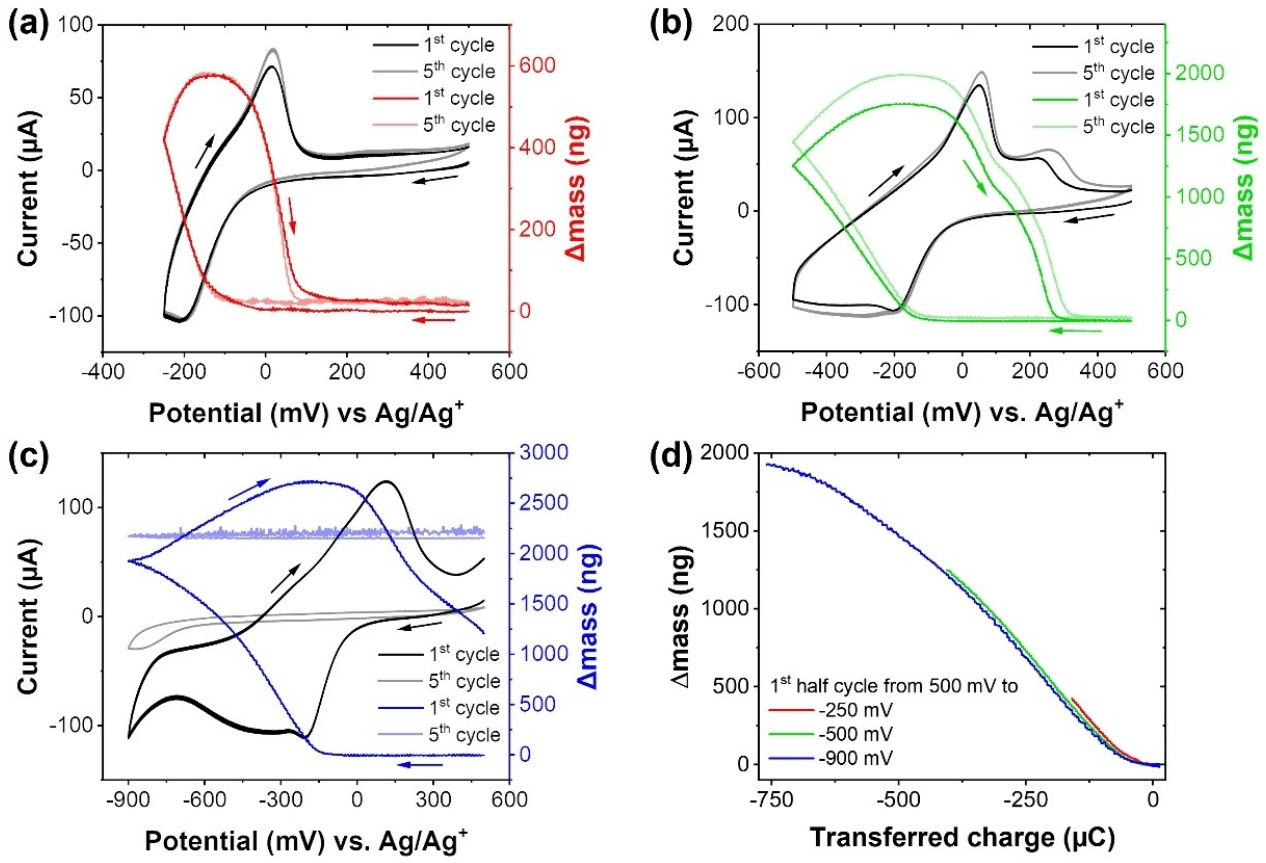

Figure 3. EQCM measurement of $K_5\{V_{12}\}$ (0.5 mM in acetonitrile containing 0.1 M $(nBu_4N)PF_6$ while using cyclic voltammetry (scan rate = 100 mV s^{-1}) in the potential ranges of **a)** 500 mV to −250 mV, **b)** 500 mV to −500 mV, and **c)** 500 mV to −900 mV vs. Ag/Ag^+ with the corresponding mass changes for the first and fifth cycle, respectively. **d)** Deposited mass vs. transferred charge during the first half cycle for the three potential ranges shown in **a)**, **b)**, and **c)**.

of 120 seconds known as deposition period (t_{on}) to induce the reduction of the clusters. The deposition period (t_{on}) and the relaxing potential (t_{off}) were repeated alternately to accomplish 10 successive reduction pulses.

The potentiostatic pulse profile at −250 mV vs. Ag/Ag^+ resulted in a gradually decreasing current response over 10 reduction pulse cycles (see Supporting Information, Figure S3), which may be associated with film formation and associated with that limited electron transfer for further reduction of the clusters. The pulse sequence with a cathodic potential of −500 mV vs. Ag/Ag^+ shows a higher reduction current, which is most likely due to the deposition of more $K_5\{V_{12}\}$ clusters and possibly additional reduction of the plated material.

Upon further decreasing the cathodic potential to −900 mV vs. Ag/Ag^+, the potentiostatic pulse profile reveals a fast decay in current response, which is assigned to a reduced electrical conductivity of the film at this potential. At the same time, a comparatively small oxidative current response shows that the deposition has become mostly irreversible, and the deposited film could not be completely re-oxidized (stripped). These findings are consistent with our EQCM results, which show irreversible POM electrodeposition when the applied potential is more negative than −500 mV vs. Ag/Ag^+. In sum, fully reversible electrodeposition of $K_5\{V_{12}\}$ is possible up to a cathodic potential of −500 mV vs. Ag/Ag^+, while irreversible electrodeposition occurs when more negative cathodic potentials are used. We hypothesized that this change of behavior could be due to chemical and/or structural changes of the deposited films at sufficiently low potentials. Thus, the thin films were characterized via scanning electron microscopy (SEM), energy dispersive X-ray spectroscopy (EDX) element mapping, Fourier transform infrared-attenuated total reflection spectroscopy (FTIR-ATR), and X-ray photoelectron spectroscopy (XPS) to elucidate the key differences of films which were pulse-deposited at the different reduction potentials (−250 mV, −500 mV and −900 mV vs. Ag/Ag^+).

Characterization of the electrodeposited thin films

SEM images of the three films deposited at −250 mV, −500 mV and −900 mV vs. Ag/Ag^+ show that uniform films with similar morphologies are formed (Supporting Information, Figure S4b–d). EDX element analyses (Supporting Information, Figure S5) reveal the presence of vanadium, potassium, oxygen, and chlorine as expected from the $K_5\{V_{12}\}$ clusters, which appear to be homogeneously distributed (Supporting Information, Figure S4b–d). To determine the film thickness and roughness (arithmetic mean height, *Sa*), atomic force microscopy (AFM) measurements were performed in acetonitrile for the three pulse-deposited films (at −250 mV, −500 mV and −900 mV vs. Ag/Ag^+). Figure 4a–c shows the topography images of the films, where defined areas of the films were partially removed to determine the film height. Especially, the deposition at −250 mV vs. Ag/Ag^+ resulted in uniform coatings with roughness values (*Sa*) of 9 ± 2 nm ($n=5$, areas of 625 μm² were evaluated), whereas films deposited at more negative potentials (−500 and −900 mV vs. Ag/Ag^+) appear less uniform ($Sa = 45 \pm 13$ nm and 32 ± 19 nm; $n=4$ and 5, respectively, areas of 625 μm² were evaluated). Extracted line profiles (Figure 4d–f) obtained from the topography images (marked with dotted lines in Figure 4a–c) show film thicknesses of 73 ± 27 nm (−250 mV vs. Ag/Ag^+), 71 ± 27 nm (−500 mV vs. Ag/Ag^+) and 37 ± 18 nm (−900 mV vs. Ag/Ag^+) ($n=30$, profiles from three different areas were evaluated, respectively).

The reduced thickness of the film deposited at −900 mV vs. Ag/Ag^+ might be attributed to the formation of a film that effectively blocks electron transfer and with that further

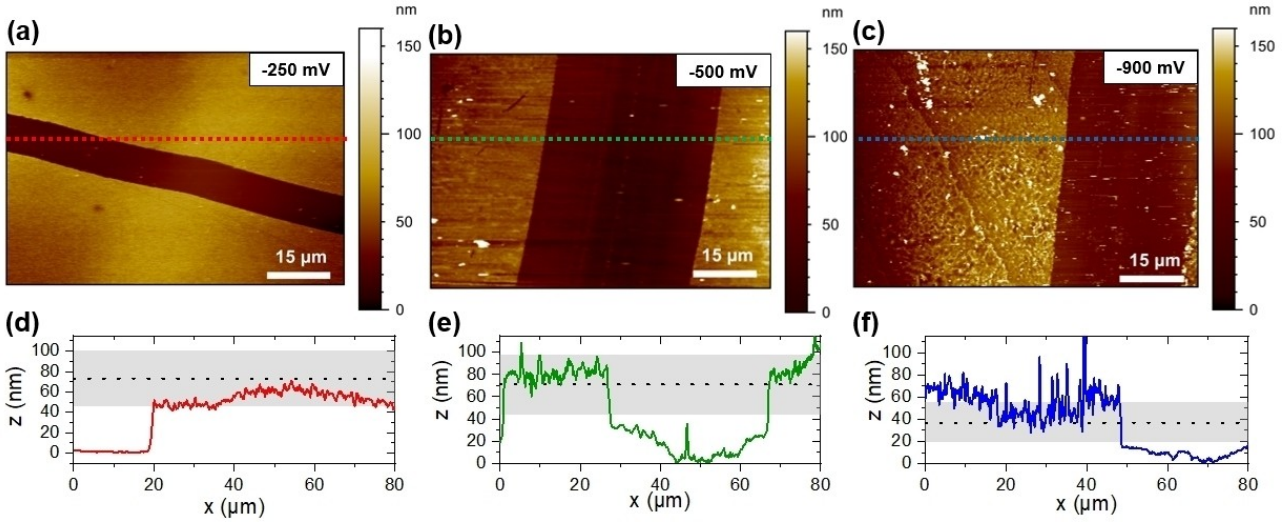

Figure 4. AFM topography images of $K_5\{V_{12}\}$ films deposited on glassy carbon via PED at **a)** −250 mV, **b)** −500 mV and **c)** −900 mV vs. Ag/Ag^+; images were recorded in contact mode in acetonitrile. Corresponding line scans **(d–f)** extracted from the topography images at the position marked by the dotted lines; dotted black lines represent average film thicknesses with standard deviations depicted as gray area ($n=30$ profiles).

deposition which is in line with the EQCM measurements. In addition, this deviating behavior compared to the other films implies a structural change of the film, which may attribute to changes in film morphology.

We also conducted FTIR-ATR spectroscopy studies to get further insights into structural integrity and possible structural changes of the $K_5\{V_{12}\}$-based films. For the films deposited at −250 mV and −500 mV vs. Ag/Ag^+, a shift of the characteristic V–O–V (820 cm^{-1}, 767 cm^{-1}, 686 cm^{-1} and 633 cm^{-1})[24] and V=O (988 cm^{-1})[24b] bands towards lower wavenumbers (by ~20 cm^{-1}) and a slight shoulder, which may originate from a peak splitting due to the further reduction of the film was observed when compared with the non-reduced, native $K_5\{V_{12}\}$ cluster (Supporting Information, Figure S6). The presence of only minor changes suggests that the $\{V_{12}\}$ molecular structure is retained, while the cluster environment (i.e., K^+ ions bound to the cluster) might be arranged in a different fashion compared to the native compound. The IR spectra of the film deposited at −900 mV vs. Ag/Ag^+ show minute differences compared to the films deposited at more positive potentials; peak shifting is less pronounced (~10 cm^{-1} towards lower wave numbers), while the splitting of the 988 cm^{-1} band still occurs. Also, new bands at 1033 cm^{-1} and 736 cm^{-1} were observed, the one at 736 cm^{-1} might indicate further structural changes of the deposited species, while the one at 1033 cm^{-1} might indicate deposition of new vanadium oxide species that could be one reason for the observed irreversibility of the electrodeposition.

Additionally, UV/Vis spectroscopy was used to probe spectral changes before and after deposition of $K_5\{V_{12}\}$. To this end, a film deposited on a glassy carbon electrode at −250 mV vs. Ag/Ag^+ was transferred to a fresh electrolyte containing 0.1 M KPF_6 (to avoid cation exchange with nBu_4N^+). The film was stripped using a pulsed potential of 500 mV vs. Ag/Ag^+ (applied for a period of total 20 minutes) resulting in re-oxidation and dissolution of the film. UV/Vis spectroscopy of the electrolyte with the stripped sample (Supporting Information, Figure S7) shows that the characteristic absorption signals of the native $K_5\{V_{12}\}$ are present in solution. This indicates that the structural integrity of $K_5\{V_{12}\}$ is retained during deposition and subsequent stripping. Also, no intervalence charge transfer bands in the Vis region were observed, indicating the complete re-oxidation of the cluster to all V^V species.[11d,21]

We further studied the films by using XPS to gain insights into the elemental composition and metal oxidation states in the deposited $K_5\{V_{12}\}$ films. Survey XPS spectra of the films deposited at −250 mV, −500 mV and −900 mV vs. Ag/Ag^+ show peaks corresponding to V, K, O, Cl, C as major components (see Supporting Information, Figure S8a). Moreover, small peaks corresponding to N and F present in the spectra originate from residual electrolyte and solvent from the electrodeposition process. XPS data for the native $K_5\{V_{12}\}$ cluster revealed the exclusive presence of V^V centers (see Supporting Information, Figure S8b). In contrast, the films electrodeposited at −250 mV and −500 mV vs. Ag/Ag^+ showed a sharp signal in the $V2p_{3/2}$ region at binding energies of ~517 eV (assigned to V^{5+}),[25] as well as weak signals at ~516 eV (indicative of V^{4+}),[26] which confirms the reduction of the cluster during the electrodeposition (Supporting Information, Figure S8c–e). For the films deposited at −250 mV vs. Ag/Ag^+, the V:K atomic ratio is 1:0.72, indicating that each $\{V_{12}\}$ cluster interacts on average with ca. 8.6 K^+ cations and resulting in an average reduction degree of 3.6 electrons per $\{V_{12}\}$ (as the native compound features five K^+ per $\{V_{12}\}$). The estimated V^{4+}:V^{5+} ratio from the curve data fitting of the $V2p_{3/2}$ is 0.3:1 indicating that the $\{V_{12}\}$ cluster is reduced on average by 3.6 electrons. The film deposited at −500 mV vs. Ag/Ag^+ showed a slightly higher V:K atomic ratio (1:0.78), corresponding to 9.4 K^+ ion per $\{V_{12}\}$, and a reduction degree of 4.4 electrons per $\{V_{12}\}$) and V^{4+}:V^{5+} ratio (0.4:1), which corresponds to a reduction degree of 4.8 electrons per $\{V_{12}\}$. These data are in excellent agreement with the EQCM results, which show that the film is further reduced following electrodeposition. The XPS data for the film deposited at −900 mV vs. Ag/Ag^+ shows the largest K^+ content (V:K, 1:0.97, corresponding to 11.6 K^+ per $\{V_{12}\}$, and a reduction degree of 6.6 electrons per $\{V_{12}\}$), which is also in line with our EQCM results, indicating further reduction processes at this potential. Surprisingly, the film deposited at −900 mV vs. Ag/Ag^+ shows the lowest V^{4+} to V^{5+} ratio (0.18:1). While current work focuses on the reversible plating and stripping of the molecular vanadium oxides, future research will also continue to study the structure of the irreversibly deposited films.

Proof-of-concept: $K_5\{V_{12}\}$ films as potential battery electrode material

To assess the storage capacity of the deposited $K_5\{V_{12}\}$ films as active cathode material in a prototype potassium-ion battery (PIB), the films deposited at −250 mV, −500 mV and −900 mV vs. Ag/Ag^+ on carbon-coated Al-foil substrates were tested via galvanostatic charge/discharge cycling in a voltage range between 1.5–3.8 V vs. K/K^+ at 50 mA g^{-1}. The film deposited at −250 mV vs. Ag/Ag^+ delivered an initial discharge capacity of 55 mAh g^{-1} (Figure 5a) which corresponds to the storage of 3.06 e^- per $K_{8.64}[V_{12}O_{32}Cl]$ (all sum formulas are derived from XPS data) according to the following equation:

$$Q = (nF)/(3.6\ M_W) = (n \cdot 26{,}800)/M_W$$

where Q is the reversible charge/discharge capacity, n is the number of electrons transferred, M_w is the molecular weight and F is the Faraday constant.

The film deposited at −500 mV vs. Ag/Ag^+ shows a slightly higher capacity of 59 mAh g^{-1}, which corresponds to the storage of 3.37 e^- per $K_{9.36}[V_{12}O_{32}Cl]$. While the film deposited at −900 mV vs. Ag/Ag^+ shows a significantly lower capacity of ~11 mAh g^{-1} (see Figure S10), which corresponds to the storage of only 0.68 e^- per $K_{11.64}$-$[V_{12}O_{32}Cl]$. This low storage capacity of the film deposited at −900 mV vs. Ag/Ag^+ might be due to the more insulating nature of the film, which effectively hinders electron trans-

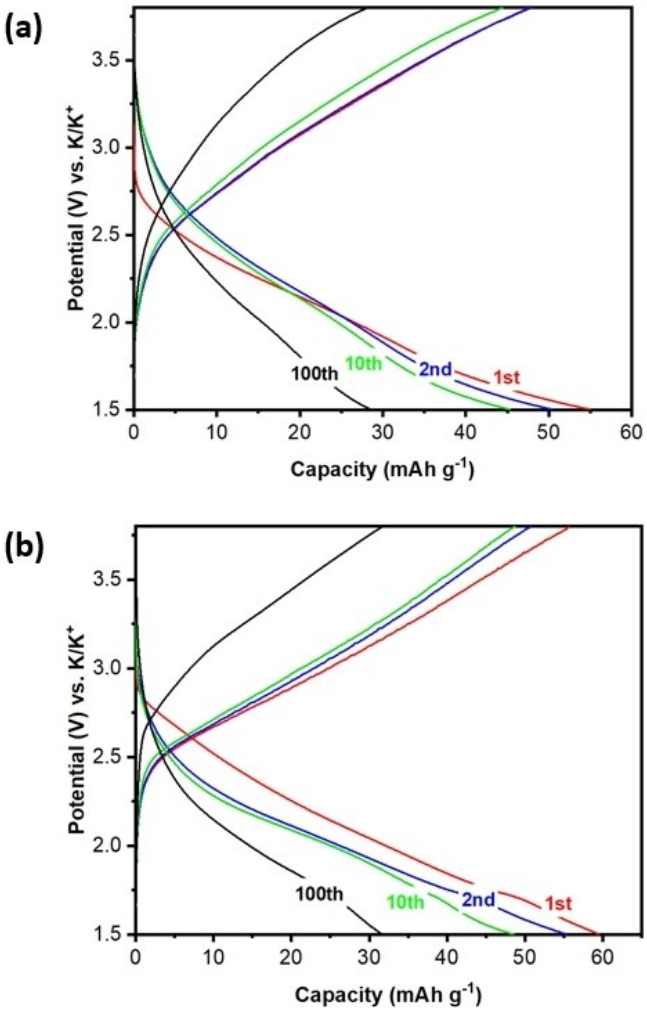

Figure 5. Selected cycles of galvanostatic cycling of the film deposited on carbon-coated Al-foil substrates at **a)** −250 mV and **b)** −500 mV vs. Ag/Ag^+ via PED; in the range of 1.5–3.8 V vs. K^+/K at 50 mA g^{-1}.

fer; again this behavior is in line with our EQCM measurements. Similarly, Pyo and co-workers previously reported the potassium-vanadium-based composite (KVP_2O_7) for high voltage cathode for PIBs and achieved the maximum discharge capacity of 60 mAh g^{-1}.[27]

All deposited films reveal a capacity fading during cycling, which might be attributed to partial dissolution of $K_5\{V_{12}\}$ into the battery electrolyte or structural rearrangements due to the intercalation/deintercalation of K^+ ions in the electrode material. Therefore, future work will focus on advanced deposition processes, targeting stable and homogeneous thin films with tunable morphology and thickness to enhance the overall capacity and address the observed capacity fading.

Conclusion

We report here the first example of reversible electrodeposition of molecular vanadium oxide clusters as a new approach towards multi-electron storage. We demonstrate that uniform films based on potassium-stabilized, reduced $\{V_{12}\}$ clusters can be formed on electrode surfaces. Within a given potential range, the deposition of the film is fully reversible, so that an electrochemical electron storage and release device can be envisaged. Mechanistic structural studies indicated that at increasingly negative deposition potentials (e.g., as shown here −900 mV vs. Ag/Ag^+), structural changes of the film occur, which affects the reversibility of the deposition process. Initial investigations of the electron storage capacity of the deposited films as future active cathode material in PIBs show promising results and will hopefully foster further investigations of this material class for electrochemical energy storage systems.

Acknowledgements

This work contributes to the research performed at CELEST (the Center for Electrochemical Energy Storage Ulm-Karlsruhe) and was funded by the Deutsche Forschungsgemeinschaft (DFG, German Research Foundation) under Germany's Excellence Strategy—EXC 2154—Project number 390874152 (POLiS Cluster of Excellence) and the TRR234 "CataLight" (project no: 364549901). Financial support by Ulm University, the Helmholtz-Gemeinschaft (HGF) is gratefully acknowledged. M. A. acknowledges the State of Baden-Württemberg for a Margarete-von-Wrangell fellowship and the Baden Württemberg Stiftung (Elite programme for Postdocs). S. G. gratefully acknowledges financial support through a Ph.D. fellowship by the Fonds der Chemischen Industrie (FCI). Dr. Thomas Diemant is acknowledged for XPS measurements. Open Access funding enabled and organized by Projekt DEAL.

Conflict of Interest

The authors declare no conflict of interest.

Data Availability Statement

The data that support the findings of this study are available from the corresponding author upon reasonable request.

Keywords: Electrochemical Quartz Microbalance · Multi-Electron Reduction · Polyoxovanadates · Pulse Electrodeposition

[1] S. Chu, A. Majumdar, *Nature* **2012**, *488*, 294–303.
[2] P. G. Bruce, B. Scrosati, J.-M. Tarascon, *Angew. Chem. Int. Ed.* **2008**, *47*, 2930–2946.
[3] F. S. da Silva, T. M. de Souza, *Int. J. Hydrogen Energy* **2017**, *42*, 26020–26036.
[4] D. G. Nocera, *Acc. Chem. Res.* **2012**, *45*, 767–776.

[5] a) A. Müller, S. Roy, *Coord. Chem. Rev.* **2003**, *245*, 153–166; b) D. L. Long, R. Tsunashima, L. Cronin, *Angew. Chem. Int. Ed.* **2010**, *49*, 1736–1758.
[6] a) H. Lv, Y. V. Geletii, C. Zhao, J. W. Vickers, G. Zhu, Z. Luo, J. Song, T. Lian, D. G. Musaev, C. L. Hill, *Chem. Soc. Rev.* **2012**, *41*, 7572–7589; b) C. Streb, *Dalton Trans.* **2012**, *41*, 1651; c) A. Sartorel, M. Carraro, F. M. Toma, M. Prato, M. Bonchio, *Energy Environ. Sci.* **2012**, *5*, 5592–5603; d) Q. Yin, J. M. Tan, C. Besson, Y. V. Geletii, D. G. Musaev, A. E. Kuznetsov, Z. Luo, K. I. Hardcastle, C. L. Hill, *Science* **2010**, *328*, 342–346.
[7] a) T. Ueda, *ChemElectroChem* **2018**, *5*, 823–838; b) Y. C. Ji, L. J. Huang, J. Hu, C. Streb, Y. F. Song, *Energy Environ. Sci.* **2015**, *8*, 776–789; c) N. Kawasaki, H. Wang, R. Nakanishi, S. Hamanaka, R. Kitaura, H. Shinohara, T. Yokoyama, H. Yoshikawa, K. Awaga, *Angew. Chem. Int. Ed.* **2011**, *50*, 3471–3474.
[8] a) M. Stuckart, K. Y. Monakhov, *Chem. Sci.* **2019**, *10*, 4364–4376; b) H. N. Miras, L. Vilà-Nadal, L. Cronin, *Chem. Soc. Rev.* **2014**, *43*, 5679–5699.
[9] M. Anjass, G. A. Lowe, C. Streb, *Angew. Chem. Int. Ed.* **2021**, *60*, 7522–7532.
[10] a) S. Greiner, M. H. Anjass, M. Fichtner, C. Streb, *Inorg. Chem. Front.* **2020**, *7*, 134–139; b) L. E. VanGelder, B. E. Petel, O. Nachtigall, G. Martinez, W. W. Brennessel, E. M. Matson, *ChemSusChem* **2018**, *11*, 4139–4149; c) K. Kastner, J. T. Margraf, T. Clark, C. Streb, *Chem. Eur. J.* **2014**, *20*, 12269–12273; d) F. Li, L. E. Vangelder, W. W. Brennessel, E. M. Matson, *Inorg. Chem.* **2016**, *55*, 7332–7334.
[11] a) F. Li, S. H. Carpenter, R. F. Higgins, M. G. Hitt, W. W. Brennessel, M. G. Ferrier, S. K. Cary, J. S. Lezama-Pacheco, J. T. Wright, B. W. Stein, M. P. Shores, M. L. Neidig, S. A. Kozimor, E. M. Matson, *Inorg. Chem.* **2017**, *56*, 7065–7080; b) R. L. Meyer, M. H. Anjass, B. E. Petel, W. W. Brennessel, C. Streb, E. M. Matson, *Chem. Eur. J.* **2020**, *26*, 9905–9914; c) L. E. VanGelder, A. M. Kosswattaarachchi, P. L. Forrestel, T. R. Cook, E. M. Matson, *Chem. Sci.* **2018**, *9*, 1692–1699; d) S. Greiner, B. Schwarz, M. Ringenberg, M. Dürr, I. Ivanovic-Burmazovic, M. Fichtner, M. Anjass, C. Streb, *Chem. Sci.* **2020**, *11*, 4450–4455.
[12] a) J. J. Chen, J. C. Ye, X. G. Zhang, M. D. Symes, S. C. Fan, D. L. Long, M. Sen Zheng, D. Y. Wu, L. Cronin, Q. F. Dong, *Adv. Energy Mater.* **2018**, *8*,1701021; b) S. Hartung, N. Bucher, H. Chen, R. Al-oweini, S. Sreejith, P. Borah, Z. Yanli, U. Kortz, U. Stimming, H. E. Hoster, M. Srinivasan, *J. Power Sources* **2015**, *288*, 270–277; c) Y. Ji, J. Hu, J. Biskupek, U. Kaiser, Y.-F. Song, C. Streb, *Chem. Eur. J.* **2017**, *23*, 16637–16643.
[13] a) B. Schwarz, J. Forster, M. K. Goetz, D. Yücel, C. Berger, T. Jacob, C. Streb, *Angew. Chem. Int. Ed.* **2016**, *55*, 6329–6333; b) B. Schwarz, J. Forster, M. H. Anjass, S. Daboss, C. Kranz, C. Streb, *Chem. Commun.* **2017**, *53*, 11576–11579.
[14] a) B. E. Petel, R. L. Meyer, M. L. Maiola, W. W. Brennessel, A. M. Müller, E. M. Matson, *J. Am. Chem. Soc.* **2020**, *142*, 1049–1056; b) E. Schreiber, B. E. Petel, E. M. Matson, *J. Am. Chem. Soc.* **2020**, *142*, 9915–9919.
[15] a) E. Schreiber, N. A. Hartley, W. W. Brennessel, T. R. Cook, J. R. McKone, E. M. Matson, *ACS Appl. Energ. Mater.* **2019**, *2*, 8985–8993; b) J. J. Chen, M. A. Barteau, *Ind. Eng. Chem. Res.* **2016**, *55*, 9857–9864; c) T. Konishi, K. Kodani, T. Hasegawa, S. Ogo, S. X. Guo, J. F. Boas, J. Zhang, A. M. Bond, T. Ueda, *Inorg. Chem.* **2020**, *59*, 10522–10531.
[16] L. Chen, M. J. Turo, M. Gembicky, R. A. Reinicke, A. M. Schimpf, *Angew. Chem. Int. Ed.* **2020**, *59*, 16609–16615.
[17] a) J. J. Chen, M. D. Symes, L. Cronin, *Nat. Chem.* **2018**, *10*, 1042–1047; b) J. J. Chen, L. Vilà-Nadal, A. Solé-Daura, G. Chisholm, T. Minato, C. Busche, T. Zhao, B. Kandasamy, A. Y. Ganin, R. M. Smith, I. Colliard, J. J. Carbó, J. M. Poblet, M. Nyman, L. Cronin, *J. Am. Chem. Soc.* **2022**, *144*, 8951–8960.
[18] A. S. Cherevan, S. P. Nandan, I. Roger, R. Liu, C. Streb, D. Eder, *Adv. Sci.* **2020**, *7*, 1903511.
[19] Z. Sun, M. Zhao, F. Li, T. Wang, L. Xu, *Mater. Res. Bull.* **2014**, *60*, 524–529.
[20] Q. Zhang, J. Ondus, J. Mills, A. Bahadori, J. Smith, T. Jordan, H. Xu, S. J. Hwu, *J. Solid State Chem.* **2020**, *287*, 121368.
[21] S. Greiner, M. Anjass, C. Streb, *CrystEngComm* **2021**, *23*, 3946–3950.
[22] a) M. H. Anjass, K. Kastner, F. Nägele, M. Ringenberg, J. F. Boas, J. Zhang, A. M. Bond, T. Jacob, C. Streb, *Angew. Chem. Int. Ed.* **2017**, *56*, 14749–14752; b) K. Kastner, M. Lechner, S. Weber, C. Streb, *ChemistrySelect* **2017**, *2*, 5542–5544; c) K. Kastner, J. Forster, H. Ida, G. N. Newton, H. Oshio, C. Streb, *Chem. Eur. J.* **2015**, *21*, 7686–7689.
[23] A. Seliverstov, C. Streb, *Chem. Eur. J.* **2014**, *20*, 9733–9738.
[24] a) H. Zhang, X. Xiao, X. Lu, G. Chai, Y. Sun, Y. Zhan, G. Xu, *J. Alloys Compd.* **2015**, *636*, 106–112; b) J. K. Li, J. Dong, C. P. Wei, S. Yang, Y. N. Chi, Y. Q. Xu, C. W. Hu, *Inorg. Chem.* **2017**, *56*, 5748–5756.
[25] E. Hryha, E. Rutqvist, L. Nyborg, *Surf. Interface Anal.* **2012**, *44*, 1022–1025.
[26] G. Silversmit, D. Depla, H. Poelman, G. B. Marin, R. De Gryse, *J. Electron Spectrosc. Relat. Phenom.* **2004**, *135*, 167–175.
[27] P. W. Bae, S. Ch. Han, Ch. Park, S. U. Hong, U. Han, S. P. Singh, Y. H. Jung, D. Ahn, K.-S. Sohn, M. Pyo, *Adv. Energy Mater.* **2017**, *8*, 1703099.

Manuscript received: May 3, 2023
Accepted manuscript online: May 22, 2023
Version of record online: July 18, 2023